Title:

Argonaute catalytic activity is required for maternal mRNA clearance in embryos

Authors: Piergiuseppe Quarato[1,2], Meetali Singh[1], Eric Cornes[1], Blaise Li[1,3], Loan Bourdon[1], Celine Didier[1], Germano Cecere[1,*]

Affiliations:

[1]Mechanisms of Epigenetic Inheritance, Department of Developmental and Stem Cell Biology, Institut Pasteur, UMR3738, CNRS, Paris, 75015 France

[2]Sorbonne Université, Collège doctoral, F-75005 Paris, France

[3]Bioinformatics and Biostatistics Hub – Department of Computational Biology, Institut Pasteur, USR 3756 , CNRS, Paris, 75015 France

[*]Corresponding author. email: germano.cecere@pasteur.fr

Abstract:

Argonaute proteins and their interacting small RNAs play a key role in regulating complementary mRNA targets during animal development. Here, we investigate a novel and essential function of the catalytically active Argonaute protein CSR-1 in maternal mRNA degradation during early embryogenesis in *Caenorhabditis elegans*. We show that CSR-1 interacts with endogenous small RNAs antisense to hundreds of cleared maternal mRNAs in embryos, and preferentially cleaves mRNAs no longer engaged in translation. The depletion of CSR-1 during maternal to zygotic transition leads to embryonic lethality in a catalytic-dependent manner and impairs the degradations of its embryonic mRNA targets. Given the conservation of Argonaute catalytic activity, we propose that a similar mechanism operate to clear maternal mRNAs during maternal to zygotic transition across species.

Main Text:

The beginning of life in animals is characterized by the transition between maternally supplied factors and the activation of the zygotic genome. The elimination of germline-produced mRNAs and proteins in somatic blastomeres and the concomitant activation of the zygotic genome during early embryonic development, is a critical step to obtain totipotent embryos (*1*). Several factors that participate in maternal mRNA clearance have been identified, including maternally-inherited PIWI-interacting RNAs (piRNAs) and zygotically-transcribed micro RNAs (miRNAs)(*2–6*), and features encoded into the mRNA sequence, such as codon optimality (*7*, *8*) RNA structures (*9*), and post-transcriptional modifications of mRNAs (*10*). In the nematode *C. elegans*, only one mechanism has been identified so far to promote maternal mRNA clearance from oocytes to 1-cell embryos (*11*). However, thousands of maternal mRNAs accumulate in the zygote and are degraded in somatic blastomeres during embryogenesis by unknown mechanisms (*12*, *13*).

Despite the role of small RNAs in maternal mRNA clearance, the requirement of the slicer activity of Argonaute proteins in maternal to zygotic transition has never been explored. In *C. elegans* the only Argonaute possessing a detectable endonucleolytic activity *in vitro* is CSR-1. CSR-1 has been mainly studied in adult worms, where it loads single-stranded small RNAs, called 22G-RNAs, generated by the RNA-dependent RNA polymerase (RdRP) EGO-1 using target germline mRNAs as a template (*14*). These 22G-RNAs are, therefore, antisense to most of the germline-expressed mRNAs and can function in protecting complementary target mRNAs from piRNAs silencing (*15–17*), promote their transcription (*18*, *19*), and fine-tune their levels through CSR-1 endonucleolytic activity (*20*). Animals lacking CSR-1 or expressing a CSR-1 catalytic inactive protein show several germline defects, severely reduced brood sizes, chromosome segregation defects, and embryonic lethality (*14*, *20*, *21*). CSR-1 and components of the CSR-1

pathway are also maternally inherited in the embryos (*14*, *20*). However, a specific function of CSR-1 during early embryogenesis remains unknown.

To precisely study the localization of CSR-1 during embryogenesis and in animal development, we have generated different CRISPR-Cas9 tagged versions of CSR-1 (*22*). As previously observed (*23*), CSR-1 is expressed mainly in the germline of adult worms and localizes in the cytoplasm and germ granules (Fig. S1 A, B). However, in early embryos, CSR-1 localizes both in germline and somatic blastomeres (Fig. 1A, and Fig. S1B). The localization of CSR-1 in the somatic blastomeres is mainly cytoplasmic and persists for several cell divisions until it becomes restricted to the perinuclear region of the germline blastomeres (Fig. 1A, and Fig. S1B). This is in contrast with other germline Argonaute proteins (*24*, *25*), such as PIWI, which exclusively segregate with the germline blastomere from the first embryonic cleavage (Fig. 1A, and Fig. S1B). To study the specific role of CSR-1 during embryogenesis, we decided to deplete CSR-1 protein specifically during oocyte and embryo production. For this purpose, we adopted the Auxin Inducible Degradation (AID) system (*26*) to trigger CSR-1 protein depletion by exposure to auxin at chosen developmental stages. We confirmed that depletion of CSR-1 starting from the first larval stage (L1) recapitulates the loss of fertility and embryonic lethality phenotypes previously observed in *csr-1 (tm892)* mutant worms (*14*) (Fig. 1B). Next, we depleted CSR-1 in adult worms starting from oogenesis (Fig. S2A). This treatment did not significantly decrease the fertility of the animals (number of eggs laid, Fig 1B), yet all the embryos failed to develop in larvae (Fig. 1C). This result suggests that CSR-1 plays an essential role during embryogenesis. To test whether the catalytic activity of CSR-1 is essential for embryonic viability, we attempted to rescue the depletion of endogenous CSR-1 with a transgenic germline expression of CSR-1. For this purpose we introduced by mosSCI (*27*), a single copy version of CSR-1 with or without an alanine substitution of the first aspartate residues within the catalytic DDH motif (Fig. 1D). While the

transgenic expression of CSR-1 catalytic dead mutant (ADH) failed to rescue the embryonic lethality caused by the oogenic specific depletion of CSR-1 (Fig. 1D), expression of a catalytic functional transgenic CSR-1 (DDH) in the same conditions rescued the embryonic lethality (Fig. 1D). These results demonstrate that CSR-1 catalytic activity is essential during embryogenesis. The peculiar localization of maternal-inherited CSR-1 in the somatic blastomeres during early embryogenesis suggests that CSR-1 and its interacting 22G-RNAs might regulate specific embryonic targets in the soma. To better understand the potential and specific regulatory function of CSR-1 in the embryo, we identified and compared CSR-1 -interacting 22G-RNAs in the embryo and adult worms. We immunoprecipitated CSR-1 in populations of embryos ranging from 1- to 20-cells stage (Fig. S3A) or young adult worms followed by RNA-seq to detect interacting 22G-RNAs complementary to mRNA targets. Our analysis revealed that even though the majority of CSR-1-22G-RNA targets in the adult germlines and early embryos largely overlap (66 %) (Fig. 2A), the relative abundance of 22G-RNAs on these targets is different between adult germlines and early embryos (Fig. 2A, B). Indeed, only 31 % of CSR-1 targets with highest levels of small RNAs (top 10 %) in adult and embryos are shared (Fig. 2A, B). Given that the impact of CSR-1 cleavage activity on target mRNAs depends on the abundance of 22G-RNAs (*20*), our results suggest that CSR-1 might regulate a different subset of mRNAs in the embryos. To evaluate gene expression changes upon CSR-1 depletion in embryos, we depleted CSR-1 in adult worms starting from the beginning of oogenesis and collected embryo populations fully depleted of CSR-1 in early stages of embryonic development (from 1-cell to 100-cell stages) (Fig. S2A and Fig. S3B). The analysis of nascent transcription by Global Run-On sequencing (GRO-seq) revealed that zygotic transcription in CSR-1 depleted embryos was largely unaffected compared to control untreated embryos (Fig. 2C), indicating that embryos were able to normally initiate zygotic transcription in the absence of CSR-1. However, the analysis of the steady-state mRNA levels by total RNA-seq

revealed increased CSR-1 embryonic mRNA targets (Fig. 2D). Moreover, the level of upregulation of these target mRNAs correlated with the levels of complementary antisense 22G-RNAs loaded into CSR-1 (Fig. 2D). These results suggest that CSR-1 directly regulates these target mRNAs at the post-transcriptional level in a dose-dependent manner. To gain insight into the type of mRNA targets regulated by CSR-1, we decided to investigate whether CSR-1 embryonic targets corresponded to the maternal or the newly transcribed zygotic mRNA transcripts. For this reason, we adapted a previously developed sorting strategy (*28*) to precisely sort populations of embryos at 1-cell stage (99 % pure), or enriched from 4- to 20-cells (early embryos), or having more than 20-cells (late embryos) (Fig. S3C). We performed stranded-specific RNA-seq on these three sorted embryo populations to profile the dynamics of gene expression during early embryonic development. Following this approach, we were able to detect 7088 maternal mRNAs inherited in 1-cell embryos (TPM > 1) (Table S1). We also identified three different classes of genes. One class of genes, which we called maternal cleared, corresponded to 1633 genes whose maternal mRNAs are inherited in 1-cell embryos and their levels gradually diminished in early and late stages (Fig. 3A) (Table S1). These genes belong to the previously characterized Maternal class II genes, which are maternally inherited in the embryos and degraded in somatic blastomeres (*12*). The second class of genes, which we called maternal stable, correspond to 1014 genes whose maternal mRNAs are inherited in 1-cell and their levels are stably maintained in early and late embryos (Fig. 3A) (Table S1). Lastly, we identified 1201 genes whose mRNAs accumulate in early and late embryos but were undetectable in 1-cell embryos (TPM < 1), suggesting that they are zygotically transcribed (Fig. 3A) (Table S1). Next, we analyzed whether the levels of embryonic CSR-1 targets followed one of these three categories of genes. Indeed, we could identify that CSR-1 embryonic mRNA targets are inherited in 1-cell embryos and gradually depleted in early and late embryos, indicating they are maternal mRNAs cleared in somatic blastomeres during embryogenesis (Fig. 3B). These

results suggest that CSR-1 can contribute to the clearance of maternal mRNAs in somatic blastomeres. To prove this, we analyzed the levels of maternal cleared mRNAs in CSR-1 depleted embryos and found reduced degradation of maternal mRNAs that are also targets of CSR-1 in the embryo (Fig. 3C). Furthermore, the accumulation of cleared maternal mRNA targets, correlates with the abundance of antisense small RNAs loaded onto CSR-1 (Fig. 3C). To demonstrate that CSR-1 is directly regulating these maternal mRNA targets in embryos, we performed RNA-seq on CSR-1 depleted embryos enriched in 1- to 4-cells stage or more advanced embryos enriched in 4- to 20 cells stage (Fig. S3E and Materials and Methods). CSR-1 depletion in 1- to 4-cell embryos did not cause global changes in the levels of maternal cleared mRNA targets. However, CSR-1 depleted embryos enriched in 4- to 20-cells showed increased levels of maternal cleared mRNA targets compared to 1- to 4-cell embryos (Fig. 3D). These results demonstrated that CSR-1 and its interacting small RNAs actively degrade their maternal mRNA targets during early embryogenesis. To confirm these results with an independent method we performed RNA Fluorescence *In Situ* Hybridization (RNA FISH) on a maternal cleared CSR-1 target in CSR-1 depleted and control embryos. As expected, we observed reduced maternal mRNA degradation of the CSR-1 target in advanced CSR-1 depleted embryos compared to control (Fig. S4). Collectively, these results suggest that the maternal inherited CSR-1 loaded with 22G-RNAs contribute to initiating the degradation of complementary maternal mRNA targets in somatic blastomeres. To better understand the dynamics of CSR-1-dependent mRNA clearance during embryogenesis, we further divided the maternal mRNA cleared genes in earlier and later degraded mRNAs. We selected 653 genes that show at least a 2-fold reduction in mRNA levels in a population of sorted embryos enriched in 4- to 20-cells compared to 1-cell embryos (earlier degraded) (Fig. 4A). Moreover, we selected 1399 genes that show stable levels of mRNAs in 4- to 20-cells compared to 1-cell embryos and that are decreased at least 2-fold in populations of embryos with more than 20 cells (later

degraded) (Fig. 4A). Because the profile of 22G-RNAs interacting with CSR-1 in the embryo has been performed in populations of embryos enriched from 1- to 20-cells, we hypothesized that CSR-1 targets would be enriched for earlier degraded maternal mRNAs. Indeed, the levels of 22G-RNAs targeting the earlier degraded mRNAs were significantly higher compared to the later degraded mRNAs in total RNAs and CSR-1 IPs (Fig. 4B, C). These results suggest that the abundance of 22G-RNAs correlates with the temporal decay of maternal cleared mRNAs during embryogenesis. We also generated metaprofiles of CSR-1-interacting 22G-RNAs levels along the gene body of earlier and later degraded target mRNAs (Fig. 4D). We observed that the 22G-RNAs loaded into CSR-1 were enriched along the whole coding sequence of the early degraded mRNAs (Fig. 4D). Instead, the later degraded mRNAs showed an enrichment of 22G-RNAs loaded into CSR-1 mainly at the 3' end of the genes in a region corresponding to the 3'UTR (Fig. 4D). Previous reports have shown that the rate of mRNA clearance during maternal to zygotic transition is influenced by translational efficiency (*7*, *8*). Thus, the different translational status of earlier and later degraded mRNAs may influence the accessibility and production of CSR-1-loaded 22G-RNAs antisense to the coding sequences of cleared mRNAs. To test this hypothesis, we measured ribosomal occupancy on maternal mRNAs by Ribo-seq in a population of embryos enriched in 4- to 20-cells (Fig. S3D). Our analysis showed that earlier degraded maternal mRNA targets have very low ribosomal occupancy and translational efficiency compared to later degraded mRNA targets (Fig. 4E, F). These results suggest that the loading of ribosomes on maternal mRNAs can influence their coding sequence accessibility for the 22G-RNA-mediated cleavage by CSR-1 in somatic blastomeres. Previous studies have shown that the codon usage of mRNAs can influence their translational efficiency and maternal mRNA decay during maternal to zygotic transition (*7*, *8*). However, the earlier and later degraded mRNAs in *C. elegans* embryos did not show any differences in their codon usage (Fig. S5). Because the translation of germline mRNAs is primarily

regulated by their 3'UTR in *C. elegans* (*29*), we decided to investigate whether different 3'UTR from earlier and later degraded mRNAs can impact the translation and the rate of mRNA degradation in early embryos. For this reason, we generated a single-copy transgene expressing a germline *mCherry::h2b* mRNA reporter with a 3'UTR from an earlier (*egg-6* 3'UTR) or later (*tbb-2* 3'UTR) degraded mRNA targets (Fig. 4G). The *mCherry::h2b* reporter fused with *egg-6* 3'UTR was indeed poorly translated in early embryos compared to *mCherry::h2b* reporter fused with *tbb-2* 3'UTR. Moreover, the level of *mCherry::h2b* mRNA reporter fused with *egg-6* 3'UTR was significantly lower in the embryos even though its level was similar in adult worms, indicating a faster rate of degradation in early embryos (Fig. 4H). To prove that CSR-1 22G-RNAs contribute to the faster decay of *mCherry::h2b* reporter fused with *egg-6* 3'UTR, we sequenced small RNAs from the two transgenic strains in early embryo preparations. Our analysis showed increased levels of small RNAs on the coding sequences of the *mCherry* transgenic reporter with *egg-6* 3'UTR compared to the one containing *tbb-2* 3'UTR (Fig. 4I, J). These results suggest that the translation level of maternal mRNAs can influence the rate of CSR-1-mediated mRNA cleavage in somatic blastomeres.

In conclusion, we have shown that the maternal inherited CSR-1 protein and its interacting 22G-RNAs trigger the cleavage of hundreds of complementary maternal mRNAs targets in somatic blastomeres. CSR-1 is the only catalytically active Argonaute protein with cleavage activity detected in *C. elegans* extract (*30*). We propose that CSR-1 catalytic activity is required during embryogenesis to cleave untranslated maternal mRNAs accumulated in somatic blastomeres after the first embryonic divisions. Catalytically active Argonaute proteins are conserved in animals, including humans. In *Drosophila* embryos, the Argonaute protein Aubergine and its interacting piRNAs have been shown to participate in maternal mRNAs clearance (*3*, *4*). However, it is still not known whether the catalytic activity of the protein is required for this process. The inheritance

of maternal Ago2, the only catalytically active Argonaute in mouse, is essential for early embryonic mouse development, and it has been suggested to play a role in maternal to zygotic transition (*31*). Moreover, endogenous small RNAs targeting protein-coding genes have been detected in the mouse oocyte and embryonic stem cells (*32–34*). Therefore, we propose that an Argonaute-mediated mRNA cleavage might be a conserved mechanism to clear maternal mRNAs during maternal to zygotic transition.

References and notes

1. V. Yartseva, A. J. Giraldez, The Maternal-to-Zygotic Transition During Vertebrate Development: A Model for Reprogramming. *Curr. Top. Dev. Biol.* **113**, 191–232 (2015).
2. A. J. Giraldez, Y. Mishima, J. Rihel, R. J. Grocock, S. Van Dongen, K. Inoue, A. J. Enright, A. F. Schier, Deadenylation and Clearance of Maternal mRNAs. **312**, 75–80 (2006).
3. B. Barckmann, S. Pierson, J. Dufourt, C. Papin, C. Armenise, F. Port, T. Grentzinger, S. Chambeyron, G. Baronian, J. P. Desvignes, T. Curk, M. Simonelig, Aubergine iCLIP Reveals piRNA-Dependent Decay of mRNAs Involved in Germ Cell Development in the Early Embryo. *Cell Rep.* **12**, 1205–1216 (2015).
4. C. Rouget, C. Papin, A. Boureux, A. C. Meunier, B. Franco, N. Robine, E. C. Lai, A. Pelisson, M. Simonelig, Maternal mRNA deadenylation and decay by the piRNA pathway in the early Drosophila embryo. *Nature*. **467**, 1128–1132 (2010).
5. E. Lund, M. Liu, R. S. Hartley, M. D. Sheets, J. E. Dahlberg, Deadenylation of maternal mRNAs mediated by miR-427 in Xenopus laevis embryos. *Rna*. **15** (2009), pp. 2351–2363.
6. N. Bushati, A. Stark, J. Brennecke, S. M. Cohen, Temporal Reciprocity of miRNAs and

Their Targets during the Maternal-to-Zygotic Transition in Drosophila. *Curr. Biol.* **18**, 501–506 (2008).

7. A. A. Bazzini, F. del Viso, M. A. Moreno-Mateos, T. G. Johnstone, C. E. Vejnar, Y. Qin, J. Yao, M. K. Khokha, A. J. Giraldez, Codon identity regulates mRNA stability and translation efficiency during the maternal-to-zygotic transition. *EMBO J.* **35**, 2087–2103 (2016).

8. Y. Mishima, Y. Tomari, Codon Usage and 3' UTR Length Determine Maternal mRNA Stability in Zebrafish. *Mol. Cell.* **61**, 874–885 (2016).

9. J. D. Beaudoin, E. M. Novoa, C. E. Vejnar, V. Yartseva, C. M. Takacs, M. Kellis, A. J. Giraldez, Analyses of mRNA structure dynamics identify embryonic gene regulatory programs. *Nat. Struct. Mol. Biol.* **25**, 677–686 (2018).

10. B. S. Zhao, X. Wang, A. V. Beadell, Z. Lu, H. Shi, A. Kuuspalu, R. K. Ho, C. He, M6 A-dependent maternal mRNA clearance facilitates zebrafish maternal-to-zygotic transition. *Nature.* **542**, 475–478 (2017).

11. M. Stoeckius, D. Grun, M. Kirchner, S. Ayoub, F. Torti, F. Piano, M. Herzog, M. Selbach, N. Rajewsky, Global characterization of the oocyte-to-embryo transition in Caenorhabditis elegans uncovers a novel mRNA clearance mechanism. *EMBO J.* **33**, 1751–1766 (2014).

12. G. Seydoux, A. Fire, Soma-germline asymmetry in the distributions of embryonic RNAs in Caenorhabditis elegans. *Development.* **120**, 2823–34 (1994).

13. L. R. Baugh, Composition and dynamics of the Caenorhabditis elegans early embryonic transcriptome. *Development.* **130**, 889–900 (2003).

14. J. M. Claycomb, P. J. Batista, K. M. Pang, W. Gu, J. J. Vasale, J. C. van Wolfswinkel, D. A. Chaves, M. Shirayama, S. Mitani, R. F. Ketting, D. Conte, C. C. Mello, The Argonaute

CSR-1 and Its 22G-RNA Cofactors Are Required for Holocentric Chromosome Segregation. *Cell*. **139**, 123–134 (2009).

15. C. J. Wedeles, M. Z. Wu, J. M. Claycomb, Protection of germline gene expression by the C. elegans argonaute CSR-1. *Dev*. *Cell*. **27**, 664–671 (2013).

16. M. Seth, M. Shirayama, W. Gu, T. Ishidate, D. Conte, C. Mello, The C. elegans CSR-1 argonaute pathway counteracts epigenetic silencing to promote germline gene expression. *Dev*. *Cell*. **27**, 656–663 (2013).

17. E. Z. Shen, H. Chen, A. R. Ozturk, S. Tu, M. Shirayama, W. Tang, Y. H. Ding, S. Y. Dai, Z. Weng, C. C. Mello, Identification of piRNA Binding Sites Reveals the Argonaute Regulatory Landscape of the C. elegans Germline. *Cell* (2018), doi:10.1016/j.cell.2018.02.002.

18. G. Cecere, S. Hoersch, S. O'keeffe, R. Sachidanandam, A. Grishok, Global effects of the CSR-1 RNA interference pathway on the transcriptional landscape. *Nat*. *Struct*. *Mol*. *Biol*. **21**, 358–365 (2014).

19. C. C. Conine, J. J. Moresco, W. Gu, M. Shirayama, D. Conte, J. R. Yates, C. C. Mello, Argonautes promote male fertility and provide a paternal memory of germline gene expression in C. Elegans. *Cell*. **155**, 1532–1544 (2013).

20. A. Gerson-Gurwitz, S. Wang, S. Sathe, R. Green, G. W. Yeo, K. Oegema, A. Desai, A Small RNA-Catalytic Argonaute Pathway Tunes Germline Transcript Levels to Ensure Embryonic Divisions. *Cell*. **165**, 396–409 (2016).

21. E. Yigit, P. J. Batista, Y. Bei, K. M. Pang, C. C. G. Chen, N. H. Tolia, L. Joshua-Tor, S. Mitani, M. J. Simard, C. C. Mello, Analysis of the C. elegans Argonaute Family Reveals that Distinct Argonautes Act Sequentially during RNAi. *Cell*. **127**, 747–757 (2006).

22. G. Barucci, E. Cornes, M. Singh, B. Li, M. Ugolini, A. Samolygo, C. Didier, F. Dingli, D. Loew, P. Quarato, G. Cecere, Small RNA-mediated transgenerational silencing of histone genes impairs fertility in piRNA mutants. *Nat. Cell Biol.*, 1–12 (2020).

23. J. C. van Wolfswinkel, J. M. Claycomb, P. J. Batista, C. C. Mello, E. Berezikov, R. F. Ketting, CDE-1 Affects Chromosome Segregation through Uridylation of CSR-1-Bound siRNAs. *Cell*. **139**, 135–148 (2009).

24. G. Wan, B. D. Fields, G. Spracklin, A. Shukla, C. M. Phillips, S. Kennedy, Spatiotemporal regulation of liquid-like condensates in epigenetic inheritance. *Nature*. **557**, 679–683 (2018).

25. J. P. T. Ouyang, A. Folkmann, L. Bernard, C. Y. Lee, U. Seroussi, A. G. Charlesworth, J. M. Claycomb, G. Seydoux, P Granules Protect RNA Interference Genes from Silencing by piRNAs. *Dev. Cell* (2019), doi:10.1016/j.devcel.2019.07.026.

26. L. Zhang, J. D. Ward, Z. Cheng, A. F. Dernburg, The auxin-inducible degradation (AID) system enables versatile conditional protein depletion in C. elegans. *Development*. **142**, 4374–4384 (2015).

27. C. Frøkjær-Jensen, M. Wayne Davis, C. E. Hopkins, B. J. Newman, J. M. Thummel, S. P. Olesen, M. Grunnet, E. M. Jorgensen, Single-copy insertion of transgenes in Caenorhabditis elegans. *Nat. Genet*. **40**, 1375–1383 (2008).

28. M. Stoeckius, J. Maaskola, T. Colombo, H. P. Rahn, M. R. Friedländer, N. Li, W. Chen, F. Piano, N. Rajewsky, Large-scale sorting of C. elegans embryos reveals the dynamics of small RNA expression. *Nat. Methods*. **6**, 745–751 (2009).

29. C. Merritt, D. Rasoloson, D. Ko, G. Seydoux, 3′ UTRs Are the Primary Regulators of Gene Expression in the C. elegans Germline. *Curr. Biol*. **18**, 1476–1482 (2008).

30. K. Aoki, H. Moriguchi, K. Okawa, H. Tabara, in *International Worm Meeting* (2007).

31. K. Lykke-andersen, M. J. Gilchrist, J. B. Grabarek, P. Das, E. Miska, M. Zernicka-goetz, <Mol. Biol. Cell-2009-Rizk-1639-51.pdf>. **19**, 4383–4392 (2008).

32. T. Watanabe, Y. Totoki, A. Toyoda, M. Kaneda, S. Kuramochi-Miyagawa, Y. Obata, H. Chiba, Y. Kohara, T. Kono, T. Nakano, M. A. Surani, Y. Sakaki, H. Sasaki, Endogenous siRNAs from naturally formed dsRNAs regulate transcripts in mouse oocytes. *Nature* (2008), doi:10.1038/nature06908.

33. O. H. Tam, A. A. Aravin, P. Stein, A. Girard, E. P. Murchison, S. Cheloufi, E. Hodges, M. Anger, R. Sachidanandam, R. M. Schultz, G. J. Hannon, Pseudogene-derived small interfering RNAs regulate gene expression in mouse oocytes. *Nature* (2008), doi:10.1038/nature06904.

34. J. E. Babiarz, J. G. Ruby, Y. Wang, D. P. Bartel, R. Blelloch, Mouse ES cells express endogenous shRNAs, siRNAs, and other microprocessor-independent, dicer-dependent small RNAs. *Genes Dev*. (2008), doi:10.1101/gad.1705308.

35. S. Brenner, THE GENETICS OF CAENORHABDITIS ELEGANS. *Genetics*. **77**, 71–94 (1974).

36. C. Frøkjær-jensen, M. W. Davis, C. E. Hopkins, B. J. Newman, J. M. Thummel, S. Olesen, M. Grunnet, E. M. Jorgensen, Single-copy insertion of transgenes in Caenorhabditis elegans. **40**, 1375–1383 (2008).

37. E. Zeiser, C. Frøkjær-Jensen, E. Jorgensen, J. Ahringer, MosSCI and gateway compatible plasmid toolkit for constitutive and inducible expression of transgenes in the c. elegans germline. *PLoS One*. **6**, 3–8 (2011).

38. L. J. Core, J. J. Waterfall, J. T. Lis, Nascent RNA sequencing reveals widespread pausing

and divergent initiation at human promoters. *Science (80-.).* **322**, 1845–1848 (2008).

39. N. Tsanov, A. Samacoits, R. Chouaib, A. M. Traboulsi, T. Gostan, C. Weber, C. Zimmer, K. Zibara, T. Walter, M. Peter, E. Bertrand, F. Mueller, SmiFISH and FISH-quant - A flexible single RNA detection approach with super-resolution capability. *Nucleic Acids Res*. **44** (2016), doi:10.1093/nar/gkw784.

40. F. Ramírez, D. P. Ryan, B. Grüning, V. Bhardwaj, F. Kilpert, A. S. Richter, S. Heyne, F. Dündar, T. Manke, deepTools2: a next generation web server for deep-sequencing data analysis. *Nucleic Acids Res*. (2016), doi:10.1093/nar/gkw257.

41. F. Aeschimann, J. Xiong, A. Arnold, C. Dieterich, H. Großhans, Transcriptome-wide measurement of ribosomal occupancy by ribosome profiling. *Methods* (2015), doi:10.1016/j.ymeth.2015.06.013.

Acknowledgements: We would like to thank all the members of the Cecere laboratory for the helpful discussion during the developing of the project. We thank Dr. Nicola Iovino for helpful discussions and suggestions on the manuscript. We thank the Miska, the Mello, and the Seydoux laboratories for sharing strains and reagents. Some strains were provided by the CGC, funded by NIH Office of Research Infrastructure Programs (P40 OD010440).

Funding: This project has received funding from the Institut Pasteur, the CNRS, and the European Research Council (ERC) under the European Union's Horizon 2020 research and innovation programme under grant agreement No ERC-StG- 679243. E.C. was supported by a Pasteur-Roux Fellowship program. P.Q. was supported by Ligue Nationale Contre le Cancer (S-FB19032).

Author contributions: G.C. identified and developed the core questions addressed in the project and analyzed the results of all experiments together with P.Q. P.Q. performed most of the experiments and helped in the analysis of the results. E.C. and L.B. generated all the CRISPR-Cas9

and MosSCI lines used in this study with the help of P.Q. M.S. performed the immunoprecipitation of CSR-1 and small RNA sequencing in adult worms and performed together with P.Q. the ribo-seq experiments. B.L. performed the bioinformatic analysis of all the sequencing data. G.C. wrote the paper with the contribution of P.Q, M.S., E.C.

Competing interests: All the authors declare no competing interests.

Data and materials availability: all the sequencing data are available upon request to the corresponding author.

Materials and Methods

C. elegans strains and maintenance

Strains were grown at 20 °C using standard methods (*35*). The wild-type reference strain used was Bristol N2. A complete list of strains used in this study is provided in Table S1.

Generation of transgenic animals

Generation of CRISPR–Cas9 lines

CRISPR-Cas9 alleles were generated as described previously (*22*). We used a *mCherry::3×Flag::ha::csr-1* (*22*) as an entry strain to introduce an auxin-inducible Degron tag and obtain a *Degron::mCherry::3xFlag::ha::csr-1* strain suitable for the auxin inducible degradation of CSR-1, after crossing with CA1352, a strain carrying a single copy of the germline expressed TIR-1 protein (*26*).

Generation of MosSCI lines

Strains carrying a single copy insertion of *mex-5P::gfp::csr-1::tbb-2 3'UTR* or *mex-5P::gfp::csr-1(ADH)::tbb-2 3'UTR* were generated by MosSCI (*36*) and the Gateway Compatible Plasmid Toolkit (*37*). The sequences of *csr-1* and *csr-1 (ADH)* were amplified from genomic DNA by PCR from strains carrying either a wild type copy of *csr-1* or *csr-1(ADH)* and cloned in pENTR-D-TOPO (Invitrogen). Plasmids used for Multisite Gateway reaction are listed as follows: pJA245, pCM1.36, pCFJ212. Strain EG6703 was used as an entry strain for single insertion in chromosome IV.

3'UTR replacement experiment

A sequence of 800bp downstream of the stop codon of egg-6 was amplified from genomic DNA by PCR and used as 3' UTR. We used the single-copy *transgene mCherry::his-11::tbb-2 3'UTR* as entry strain to insert *egg-6 3'UTR* by CRISPR-Cas9 as described above. *egg-6 3'UTR* was inserted right after the STOP codon of *his-11*. The specific expression of the inserted UTR was validated by RT-qPCR.

Immunostaining

Gonads were dissected on PBS, 0.1 % Tween-20 (PBST) containing 0.3 mM levamisole on 0.01 % poly-lysine slides. Samples were immediately freeze cracked on dry ice for 10 min and fixed at −20°C for 15 min in methanol, and 10 min in acetone. Blocking (30 minutes at room temperature) and antibody incubations (primary, overnight at 4°C; secondary 1 hour at room temperature) was performed in 1×PBS, 0.1 % Tween-20, 5 % BSA. Washes were performed with 1×PBS, 0.1 % Tween-20 (PBST). DNA was stained with DAPI. For embryo immunostaining, a drop of embryos from bleached adults was used instead of gonads.

Auxin-inducible depletion of CSR-1

Auxin-inducible depletion has been performed as described in (*26*). 250 mM Auxin stock solution was prepared in Ethanol and stored at 4°C. Auxin plates or Ethanol plates were prepared by the addition of Auxin or only Ethanol to NGM plates (final concentration: 500 µM auxin, 0.5 % Ethanol for Auxin plates and 0.5 % Ethanol for Ethanol plates). Plates were seeded with OP50 *E. Coli*, stored at 4°C and warmed at room temperature before the experiment. Worms were placed on Auxin or Ethanol plates from L1 or at the beginning of oogenesis as explained for each experiment.

Brood size assays

WT and CSR-1 mutants

Single L1 larvae were manually picked and placed onto NGM plates seeded with OP50 *E. coli* and grown at 20°C until adulthood and then transferred on a new plate every 24 hours for a total of 2 transfers. The brood size of each worm was calculated by counting the number of embryos and larvae laid on the 3 plates. For the auxin-depleted experiments NGM plates were supplemented with Ethanol (control) or Auxin.

Brood size of CSR-1 auxin-depleted worms during oogenesis

For CSR-1 depletion during oogenesis: brood size assay has been performed as described above with the exception that worms were grown from L1 on regular NGM plates and transferred onto Auxin or Ethanol plates 44h after hatching and transferred on new corresponding Auxin and Ethanol plates every 24 hours for a total of 2 transfers.

Embryonic lethality assay of CSR-1 rescue experiments

Single L1 larvae of strains carrying Degron::CSR-1 complemented with the single-copy insertion Mex-5P::GFP::CSR-1::tbb-2 3'UTR or Mex-5P::GFP::CSR-1(ADH)::tbb-2 3'UTR were manually picked and placed onto NGM plates seeded with OP50 *E. coli* and grown at 20°C until adulthood. Since transgene was prone to silencing, adult worms were allowed to lay at least 65 embryos and then adults were removed from the plates and imaged to check for GFP::CSR-1 expression. Only plates from GFP expressing adults were used for the assay. The percentage of embryonic lethality is calculated by dividing the number of dead embryos for the total number of laid embryos.

Collection of early embryos populations

Synchronous populations of worms were grown on NGM plates until adulthood and were carefully monitored using a stereomicroscope and bleached shortly after worms started to produce the first embryos. After bleaching, Early embryos were washed with cold M9 buffer to slow down embryonic development and immediately frozen in dry ice. A small aliquot of embryo pellet (2 µL) was taken right before freezing and mixed with 10 µL VECTASHIELD® Antifade Mounting Medium with DAPI (Vector laboratories) and immediately frozen in dry ice. DAPI stained embryos were defrosted on ice and used for counting cell nuclei and score the embryonic cell stage of the population.

Collection of CSR-1 depleted early embryos populations

Early embryos were collected as described above with the exception that worms were transferred on Auxin or Ethanol plates at the beginning of oogenesis.

Collection of early and late CSR-1 depleted embryo populations

Early populations of CSR-1 depleted embryos were collected as described above with the exception that harvesting was performed at the very beginning of embryo production to further enrich the population in early staged embryos. After bleaching, an aliquot of the same population was allowed to develop further for 1 to 2h in M9 containing 500 µM Auxin, 0.5 % Ethanol or 0.5 % Ethanol. Embryonic cell stage was scored, and harvesting was performed when embryo populations reached the desired developmental stage.

sRNA-seq library preparation

Total RNA from staged embryo preparations with RIN>9 was used to generate sRNA libraries as previously described (*22*).

RNA IP

A synchronous population of 40,000 worms (48h after hatching) or a preparation of at least 150,000 early embryos was collected and suspended in extraction buffer (50 mM HEPES pH 7.5, 300 mM NaCl, 5 mM $MgCl_2$, 10 % glycerol, 0.25 % NP-40, protease inhibitor cocktails (Thermo Scientific), 40 U/mL RiboLock RNase inhibitors (Thermo Scientific)). Samples were crushed in a metal dounce on ice performing at least 40 strokes. Crude protein extracts were centrifuged at 12,000 rpm at 4°C for 10 minutes. Protein was quantified using Pierce™ 660 nm Protein Assay Reagent (Thermo Scientific) and 1 mg (for adults) or 700 µg (for embryos) of protein extract was used for RNA immunoprecipitation as described in (*22*) and used for sRNA-seq library preparation.

GRO-seq on CSR-1 depleted embryos:

Populations containing at least 40,000 CSR-1 depleted early embryos were collected as described above. Early embryos were resuspended in 1,5mL Nuclei extraction buffer (3 mM $CaCl_2$, 2 mM $MgCl_2$, 10 mM Tris HCl pH 7.5, 0.25 % Np-40, 10 % Glycerol, Protease inhibitors and RNase inhibitor 4U/mL) and transferred to a steel dounce and stroked 40 times. The lysate was cleared from cell debris by centrifuging at 100g and nuclei were pellet at 1000g and washed 4 times with Nuclei extraction buffer. Nuclei were washed once with Freezing buffer (50 mM Tris HCl pH 8, 5 mM $MgCl_2$, 0.1 mM EDTA) and resuspended in 100 µL Freezing buffer.

Nuclear Run-On reaction and RNA extraction

Nuclear Run-On reaction was performed by addition of 100 µL NRO 2x buffer (10 mM Tris HCl, 5 mM $MgCl_2$, 1 mM DTT, 300 mM KCl, 1 % Sarkosyl, 0.5 mM ATP, CTP and GTP and 0.8 U/µL RNase inhibitor) and using 1 mM Bio-11-UTP final concentration and incubation for 5 minutes at 30°C. NRO reaction was stopped by the addition of TRIzol LS reagent (Ambion) and RNA

extraction was performed following the manufacturer's instructions. Purified RNA was fragmented by the addition of reverse transcriptase buffer and incubation for 7 minutes at 95°C.

Biotin RNA enrichment

Biotinylated nascent RNAs were bound to 30 µL Dynabeads MyOne Streptavidin C1 (Invitrogen and) washed 3 times as described in (*38*) and purified with TRIZOL reagent.

RNA 5'-end repair

5'-OH or fragmented RNAs were repaired using Polynucleotide kinase (Thermo scientific) following manufacturer instructions and incubated at 37˚C for 30 minutes. RNA was purified with Phenol:Chloroform and precipitated by the addition of 3 volumes of Ethanol, 1/10 volumes of 3 M Sodium Acetate and 30 µg Glycoblue coprecipitant (Ambion).

Ligation of 3' and 5' Adapter Oligos and 2nd and 3rd Biotin enrichments

RNA was ligated to 3' end adapter using T4 RNA ligase 2 Truncated KQ (home-made) for 16h at 15˚C. After ligation RNA was purified using solid-phase reversible immobilization beads (SPRI beads) and biotinylated RNA was enriched as described above. After purification RNA was ligated at 5' end using T4 RNA ligase 1 for 2 h at 25˚C. RNA was purified using SPRI beads and biotinylated RNA was enriched for a third time as described above.

Reverse transcription and amplification of cDNA libraries

Purified RNA was reverse transcribed using SuperScript IV Reverse Transcriptase (Thermo Fisher Scientific) following manufacturer conditions except that reaction was incubated for 1h at 50˚C. cDNA was PCR amplified with specific primers using Phusion High fidelity PCR master mix 2x (New England Biolab) for 18-20 cycles and sequenced on Illumina Next 500 system.

Sorting of *C. elegans* embryos

Sorting of *C. elegans* embryos was performed as described in (*28*) with the following modifications: a strain expressing both mCherry::OMA-1 and PIE-1::GFP was used to collect embryos at three different developmental stages (see Fig. S3C); embryos after bleaching were fixed with 2% formaldehyde in M9 to block cell division. After sorting, embryos were reverse crosslinked in 250µL RIPA buffer with RNase inhibitors for 30 minutes at 70°C and RNA was extracted with TRIzol LS (Ambion) following manufacturer instructions.

Strand-specific RNA-seq library preparation

Strand-specific RNA-seq libraries were prepared as described previously (*22*).

RT-qPCR

1 µg DNase treated total RNA was used as a template for cDNA synthesis using random hexamers and M-MLV reverse transcriptase. qPCR reaction was performed using Applied Biosystems Power up SYBR Green PCR Master mix following the manufacturer's instructions and using an Applied Biosystems QuantStudio 3 Real-Time PCR System. Primers used for qPCR are listed in Table S1.

Single-molecule inexpensive FISH

Single-molecule inexpensive FISH (smiFISH) was performed as described in (*39*). Briefly, embryos were harvested by bleaching, immediately resuspended in Methanol at -20˚C, freeze cracked in liquid nitrogen for 1 minute and incubated at -20˚C overnight. Embryos were washed once in wash buffer (10 % formamide, 2x SSC buffer (Ambion)) and hybridized with the corresponding FLAP containing probes in 100µL hybridization buffer (10 % dextran sulfate, 2 mM vanadyl-ribonucleoside complex, 0.02 % RNAse-free BSA, 50 µg *E. coli* tRNA, 2xSSC, 10 % formamide) at 30˚C overnight. Hybridized embryos were washed twice with wash buffer and once

in 2x SSC buffer before imaging. Right before imaging, embryos were resuspended in 100µL anti-fade buffer (0.4 % glucose, 10 µM Tris-HCl pH8, 2x SSC) with 1µL catalase (Sigma-Aldrich) and 1 µL glucose oxidase (3.7 mg/mL, Sigma-Aldrich) and stained with VECTASHIELD® Antifade Mounting Medium with DAPI (Vector laboratories). Images were taken using a Zeiss LSM 700 confocal microscopy.

Sequencing data analyses

Analysis for RNA-seq, sRNA-seq, and GRO-seq have been performed as previously described (*22*). Metaprofiles were generated using RPM from sRNA-seq analysis by summarizing normalized coverage information (taken from bigwig files and averaged across replicates) along early degraded targets or late degraded targets using deeptools (*40*).

Ribo-seq

Ribo-seq have been performed as described in (*41*) with some modifications. Briefly, embryos harvested by bleaching were lysate in Polysome buffer and fractionated on sucrose gradient by ultracentrifugation. RNA from monosome fraction was Dnase treated and fragments of 28-30 nucleotides were size selected after running on a TBE-Urea gel 15%. 28-30 Ribosome protected fragments were cloned with the previously described sRNA-seq library preparation approach with the following modifications: 3'phosphate was removed and 5' end was phosphorylated by treating RNA with Polynucleotide kinase.

RSCU calculation

RSCU for earlier and later degraded mRNAs was calculated using CAI calculator (http://genomes.urv.es/CAIcal/).

Gene lists

Gene lists are provided in Table S1.

Figure Legends:

Fig. 1. CSR-1 localizes to the cytoplasm of somatic blastomeres and is essential for embryonic development.

(A) Immunostaining of CSR-1 and PIWI in 1-cell, 4-cells, 8 cells, and more than 100-cells embryo, in 3xFLAG::HA::CSR-1 CRISPR-Cas9 strain using α-FLAG and α-PRG-1 antibodies. PIWI mainly localizes to the germline blastomere. CSR-1 localizes also in the cytoplasm of somatic blastomeres until it become exclusively expressed in germline blastomeres in 100-cells embryos **(B)** Brood sizes assay of *csr-1(tm892)* mutant and CSR-1 degron strains with and without Auxin. Dots correspond to the total number of eggs laid from individual worms. The black lines indicate the mean, the error bars the standard deviation is indicated in parenthesis. **(C)** Percentage of embryonic lethality from the brood size experiment shown in **(B)**, measured as the percentage of dead embryos versus the total number of laid embryos. **(D)** Percentage of embryonic lethality in CSR-1 degron strains complemented with single-copy transgenic expression of CSR-1 with (ADH) or without (DDH) mutation in the catalytic domain. The percentage of embryonic lethality is calculated by dividing the number of dead embryos from the total number of laid embryos. Dots correspond to the percentage of embryonic lethality from individual worms. The graphical representation of the experiment is shown on the left.

Fig. 2. CSR-1 regulates a different set of targets in the embryo at the post-transcriptional level.

(A) The comparison of the total, top 50 %, or top 10 % of CSR-1 targets in adults and the early embryo is shown. CSR-1 targets have been calculated as the log2 fold change >1 of the ratio between normalized 22G-RNAs from CSR-1 immunoprecipitation and the total RNA input **(B)** Genomic view of two CSR-1 target genes showing normalized 22G-RNAs in CSR-1 IPs from adult

(top) or early embryos (bottom). *glh-1* and *cpg-1* belong to the top 10 % of CSR-1 targets in adults and embryos respectively. **(C)** Box plots showing the $\log_2$ fold change of nascent RNAs (by GRO-seq) in CSR-1 depleted early embryos compared to control. The total, top 50 %, or top 10 % of CSR-1 embryonic targets are shown. Box plots display median (line), first and third quartiles (box) and highest/lowest value (whiskers). The cell stage of the embryonic population used is shown in Fig. S3B. **(D)** Box plots showing the $\log_2$ fold change of mRNAs (by RNA-seq) in CSR-1 depleted early embryos compared to control. The total, top 50 %, or top 10 % of CSR-1 embryonic targets are shown. Box plots display median (line), first and third quartiles (box) and highest/lowest value (whiskers). The cell stage of the embryonic population used is shown in Fig. S3B.

Fig. 3. CSR-1 embryonic targets correspond to cleared maternal mRNAs.

(A) Detection of maternal cleared mRNAs, stable mRNAs, or zygotic mRNAs by RNA-seq from sorted 1-cell stage, early stage, and late stage embryos. Median levels and 95% confident interval of normalized reads are shown. The stage of the three sorted embryonic population for RNA-seq is shown in Fig. S3C. **(B)** mRNA levels of CSR-1 embryonic targets in sorted embryonic populations shown in **(A)**. Median levels and 95% confident interval of normalized reads are shown. The stage of the three sorted embryonic population for RNA-seq is shown in Fig. S3C. **(C)** Cumulative distribution of the $\log_2$ fold change of maternal cleared mRNAs in CSR-1 depleted early embryos compared to control. The total, top 50 %, or top 10 % of CSR-1 embryonic targets are shown. The cell stage of the embryonic population used is shown in Fig. S3B. **(D)** Cumulative distribution of the $\log_2$ fold change of top 50 % maternal cleared mRNAs in CSR-1 depleted early embryos compared to CSR-1 depleted late embryos. The cell stage of the embryonic population used is shown in Fig. S3E.

Fig. 4. CSR-1 preferentially cleaves maternal mRNAs unloaded of ribosomes.

(A) Detection of earlier and later maternal cleared mRNAs by RNA-seq from sorted 1-cell stage, early stage, and late stage embryos. Median levels and 95 % confident interval of normalized reads are shown. The stages of the three sorted embryonic population for RNA-seq are shown in Fig. S3C. **(B) and (C)** Abundance of CSR-1-bound 22G-RNAs (B) or total 22G-RNAs (C) antisense to earlier and later maternal cleared mRNAs. Median levels and 95 % confident interval of normalized 22G-RNA reads are shown. **(D)** Metaprofile analysis showing the distribution of normalized 22G-RNA reads (RPM) across CSR-1 earlier (orange) and later (blue) maternal cleared mRNAs targets in CSR-1 immunoprecipitation (IP) or total RNA input. TSS indicates the transcriptional start site, TTS indicates the transcriptional termination site. **(E)** Ribosomal occupancy (by ribo-seq) of earlier and later maternal cleared mRNAs in early embryo preparations. Median levels and 95 % confident interval of normalized ribosomal protected fragment (RPF) reads. The stage of the embryonic population is shown in Fig. S3D. (F) Translational efficiency of earlier and later maternal cleared mRNAs in early embryo preparations. The stage of the embryonic population is shown in Fig. S3D. **(G)** Schematic of the two single-copy MosSci transgenic reporters with germline expressed mCherry::H2B fused to 3'UTR derived from earlier (egg-6 3'UTR) or later (tbb-2 3'UTR) maternal cleared mRNAs. **(H)** Reverse Transcriptase and quantitative PCR (RT-qPCR) assay to detect mRNAs from the two transgenic reporters described in **(G)**. **(I)** Quantification of 22G-RNA normalized reads per million (RPM) antisense to the mCherry sequence from the two transgenic reporters described in **(G)**. **(J)** Genomic view of normalized reads 22G-RNAs antisense to mCherry sequence from the two transgenic reporters described in **(G)**.

Fig. S1.

(A) Immunostaining of CSR-1 in adult dissected gonads in 3xF:AG::HA::CSR-1 CRISPR-Cas9 strain using α-FLAG antibody. **(B)** Immunostaining of CSR-1 and PIWI in dissected gonads (top images) and 1-cell, 4-cells, 8 cells, and more than 100-cells embryo (bottom images) as shown in Fig. 1A using α-FLAG and α-PRG-1 antibodies. Scale bar represent 10µm.

Fig. S2.

(A) DIC micrographs (left) and fluorescent micrographs (right) of live animals expressing Degron::mCherry::3xFLAG::HA::CSR-1 used for auxin depletion experiments (see Materials and methods). Top images show animals before the treatment. Bottom images show gravid animals after treatment with ethanol (no auxin, control) or auxin. Auxin treatment completely deplete CSR-1 in adult gonads and embryos. Dashed lines represent gonads or embryos. All scale bars represent 10 µm.

Fig. S3.

Composition of embryo populations used for sequencing experiments. Embryos were stained with DAPI and frozen to stop cell division (see Material and Methods). Number of nuclei in at least 100 embryos were counted using a fluorescent microscope. **(A)** 3xFLAG::HA::CSR-1 embryos used for small RNA-seq in **Fig 2A, B**. **(B)** Degron::mCherry::3xFLAG::HA::CSR-1 embryos treated with auxin or ethanol (No Auxin) used for GRO-seq and RNA-seq in **Fig 2C, D**. **(C)** Embryos expressing OMA-1::mCherry; PIE-1::GFP embryos used for sorting 1-cell, early and late embryo populations for RNA-seq in **Fig. 3A**. **(D)** *Wild-type* embryos used for Ribo-seq in **Fig 4F**. **(E)** Degron::mCherry::3xFLAG::HA::CSR-1 embryos treated with auxin or ethanol (No Auxin) used for RNA-seq of early and late embryos in **Fig 3D**. All graphs show mean of replicates with standard deviation.

Fig. S4.

smFISH showing *oma-1* mRNA levels in CSR-1 depleted embryos (right) or control embryos (left) at 1-cell stage (top) or more advanced embryos (26-48 cell stage, bottom). CSR-1 depleted embryos accumulate higher levels of the cleared maternal mRNA target *oma-1* at later stages of embryonic development compared to control embryos. Blue: DAPI; red: *oma-1* mRNA. Dashed lines represent embryos' outline.

Fig. S5.

(A) Relative synonymous codon usage (RSCU) of earlier degraded mRNAs (top) or later degraded mRNAs (bottom). Bars show mean with 95% confidential interval. **(B)** Average RSCU for each codon in earlier degraded mRNAs or later degraded mRNAs.

Fig. 1

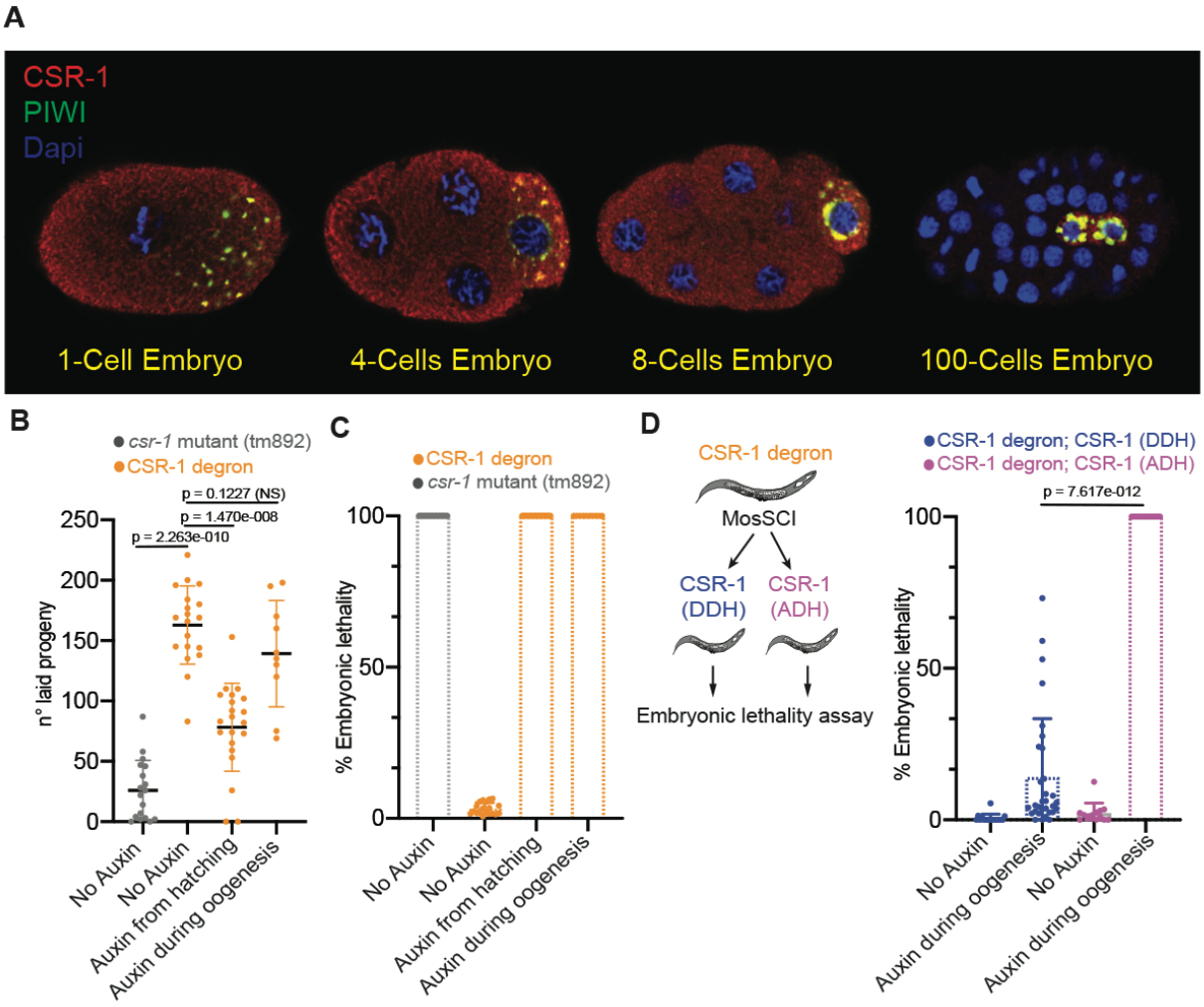
A
CSR-1
PIWI
Dapi
1-Cell Embryo
4-Cells Embryo
8-Cells Embryo
100-Cells Embryo
B
csr-1 mutant (tm892)
CSR-1 degron
p = 0.1227 (NS)
p = 1.470e-008
p = 2.263e-010
n° laid progeny
250
200
150
100
50
0
No Auxin
No Auxin
Auxin from hatching
Auxin during oogenesis
C
CSR-1 degron
csr-1 mutant (tm892)
% Embryonic lethality
100
50
0
No Auxin
No Auxin
Auxin from hatching
Auxin during oogenesis
D
CSR-1 degron
MosSCI
CSR-1 (DDH)
CSR-1 (ADH)
Embryonic lethality assay
CSR-1 degron; CSR-1 (DDH)
CSR-1 degron; CSR-1 (ADH)
p = 7.617e-012
% Embryonic lethality
100
50
0
No Auxin
Auxin during oogenesis
No Auxin
Auxin during oogenesis

Fig. 2

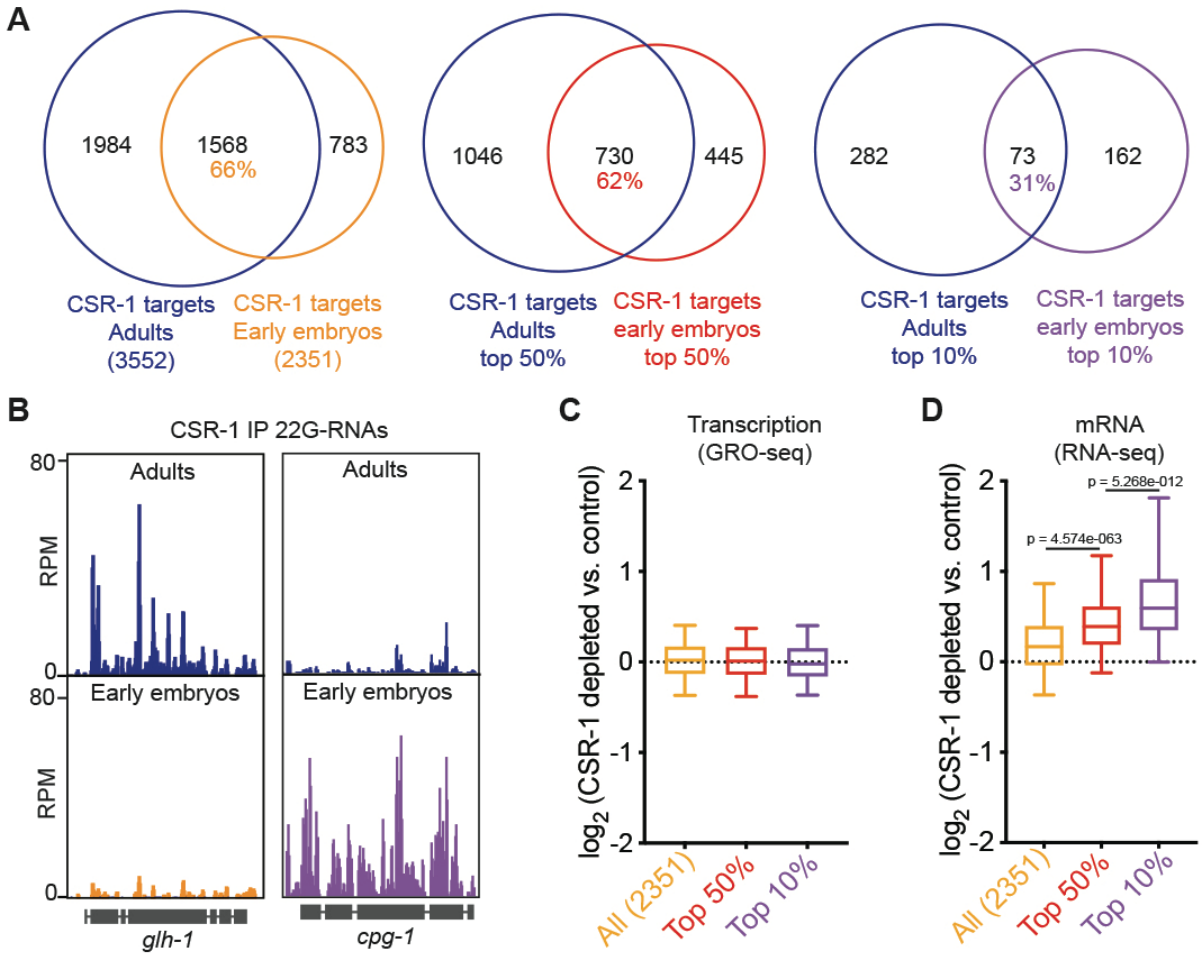
A
1984
1568
66%
783
CSR-1 targets
Adults
(3552)
CSR-1 targets
Early embryos
(2351)
1046
730
62%
445
CSR-1 targets
Adults
top 50%
CSR-1 targets
early embryos
top 50%
282
73
31%
162
CSR-1 targets
Adults
top 10%
CSR-1 targets
early embryos
top 10%
B
CSR-1 IP 22G-RNAs
Adults
Adults
Early embryos
Early embryos
RPM
80
0
glh-1
cpg-1
C
Transcription
(GRO-seq)
log2 (CSR-1 depleted vs. control)
2
1
0
-1
-2
All (2351)
Top 50%
Top 10%
D
mRNA
(RNA-seq)
p = 4.574e-063
p = 5.268e-012
log2 (CSR-1 depleted vs. control)
All (2351)
Top 50%
Top 10%

Fig. 3

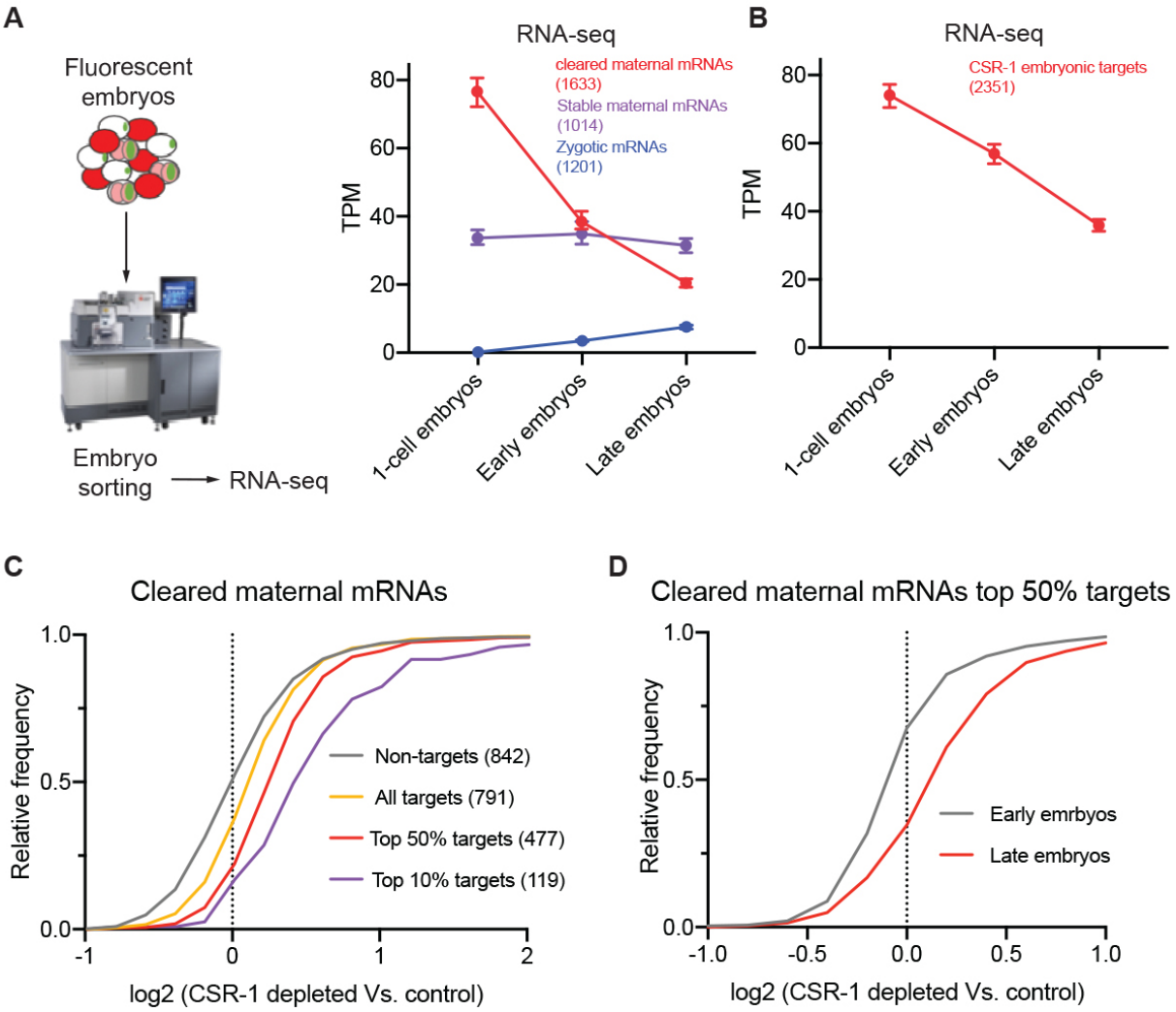
A
Fluorescent embryos
Embryo sorting
RNA-seq
RNA-seq
cleared maternal mRNAs (1633)
Stable maternal mRNAs (1014)
Zygotic mRNAs (1201)
TPM
80
60
40
20
0
1-cell embryos
Early embryos
Late embryos
B
RNA-seq
CSR-1 embryonic targets (2351)
TPM
80
60
40
20
0
1-cell embryos
Early embryos
Late embryos
C
Cleared maternal mRNAs
Relative frequency
1.0
0.5
0.0
-1
0
1
2
log2 (CSR-1 depleted Vs. control)
Non-targets (842)
All targets (791)
Top 50% targets (477)
Top 10% targets (119)
D
Cleared maternal mRNAs top 50% targets
Relative frequency
1.0
0.5
0.0
-1.0
-0.5
0.0
0.5
1.0
log2 (CSR-1 depleted Vs. control)
Early emrbyos
Late embryos

Fig. 4

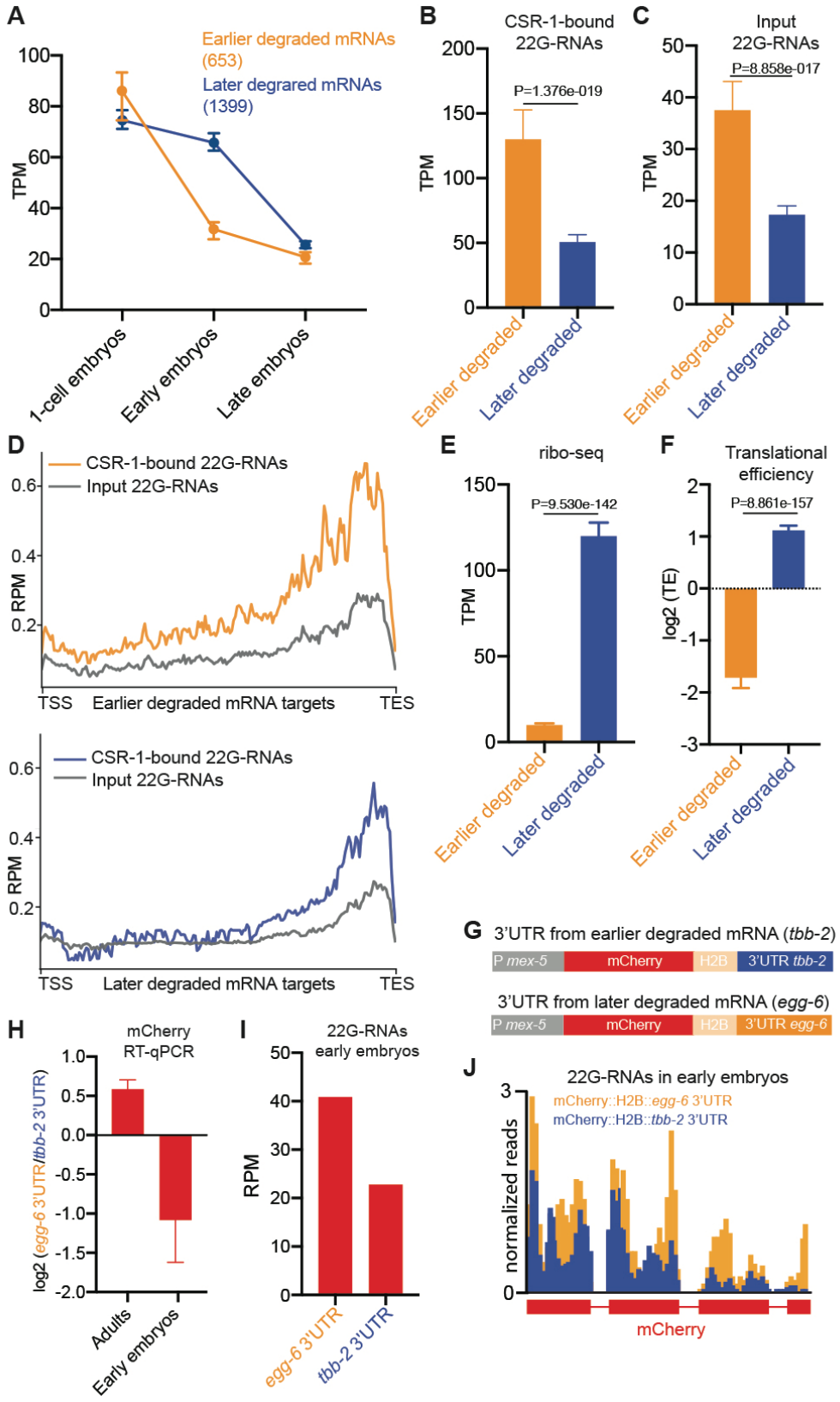
A
Earlier degraded mRNAs (653)
Later degrared mRNAs (1399)
TPM
1-cell embryos
Early embryos
Late embryos
B
CSR-1-bound 22G-RNAs
P=1.376e-019
TPM
Earlier degraded
Later degraded
C
Input 22G-RNAs
P=8.858e-017
TPM
Earlier degraded
Later degraded
D
CSR-1-bound 22G-RNAs
Input 22G-RNAs
RPM
TSS
Earlier degraded mRNA targets
TES
CSR-1-bound 22G-RNAs
Input 22G-RNAs
RPM
TSS
Later degraded mRNA targets
TES
E
ribo-seq
P=9.530e-142
TPM
Earlier degraded
Later degraded
F
Translational efficiency
P=8.861e-157
log2 (TE)
Earlier degraded
Later degraded
G
3'UTR from earlier degraded mRNA (tbb-2)
P mex-5
mCherry
H2B
3'UTR tbb-2
3'UTR from later degraded mRNA (egg-6)
P mex-5
mCherry
H2B
3'UTR egg-6
H
mCherry RT-qPCR
log2 (egg-6 3'UTR/tbb-2 3'UTR)
Adults
Early embryos
I
22G-RNAs early embryos
RPM
egg-6 3'UTR
tbb-2 3'UTR
J
22G-RNAs in early embryos
mCherry::H2B::egg-6 3'UTR
mCherry::H2B::tbb-2 3'UTR
normalized reads
mCherry

Fig. S1

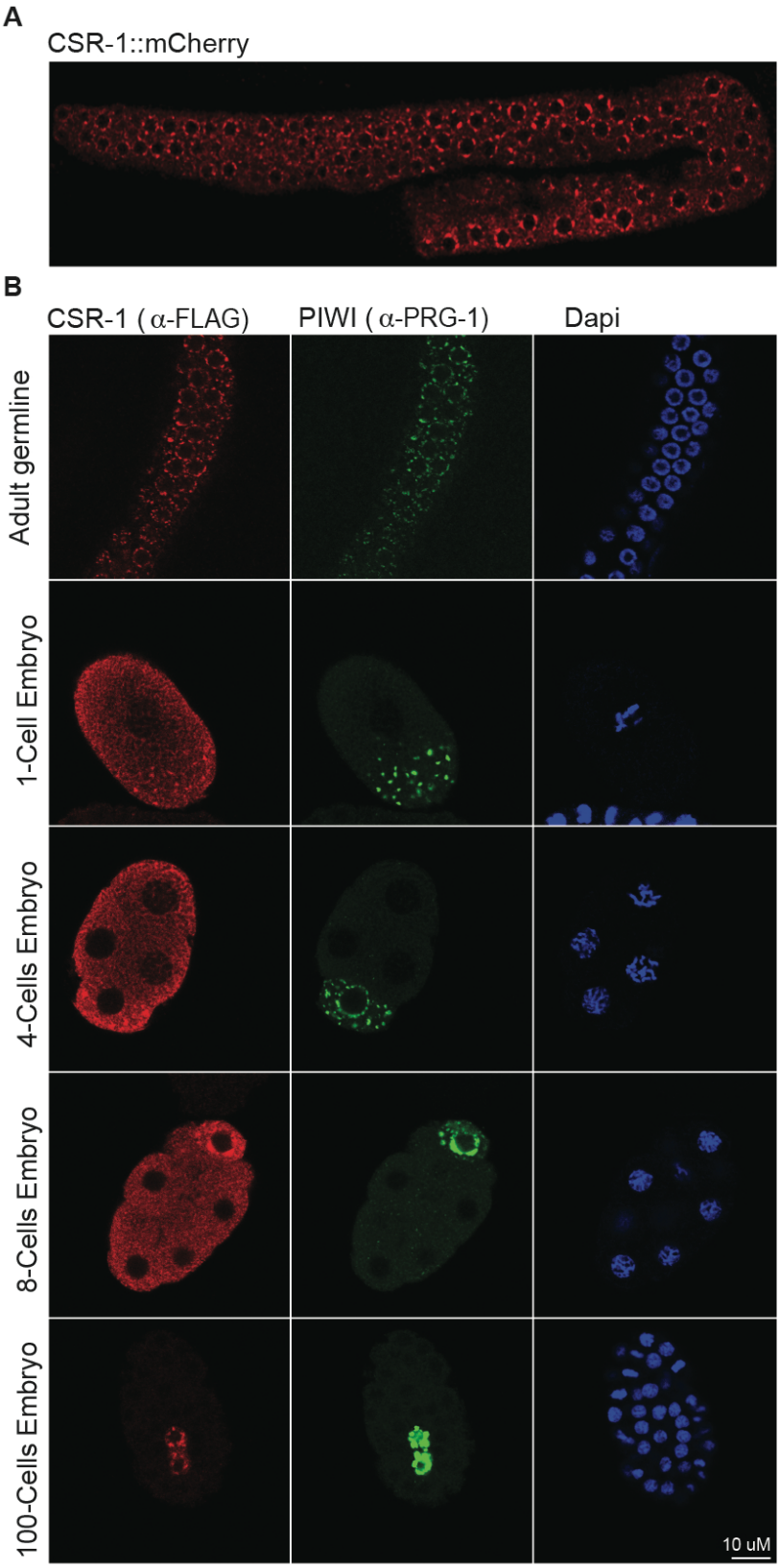
A
CSR-1::mCherry
B
CSR-1 (α-FLAG)
PIWI (α-PRG-1)
Dapi
Adult germline
1-Cell Embryo
4-Cells Embryo
8-Cells Embryo
100-Cells Embryo
10 uM

Fig. S2

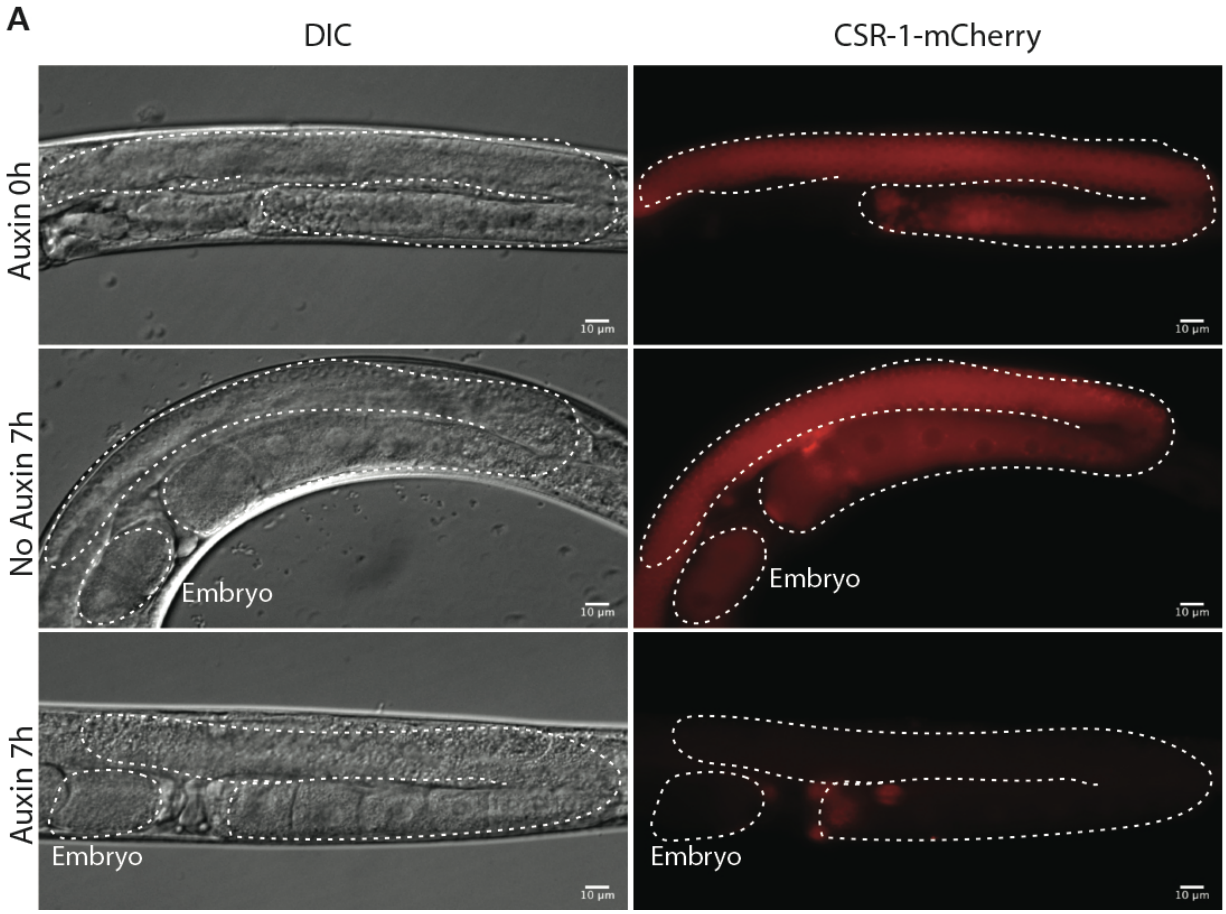
A
DIC
CSR-1-mCherry
Auxin 0h
No Auxin 7h
Auxin 7h
Embryo
Embryo
Embryo
Embryo
10 µm

Fig. S3

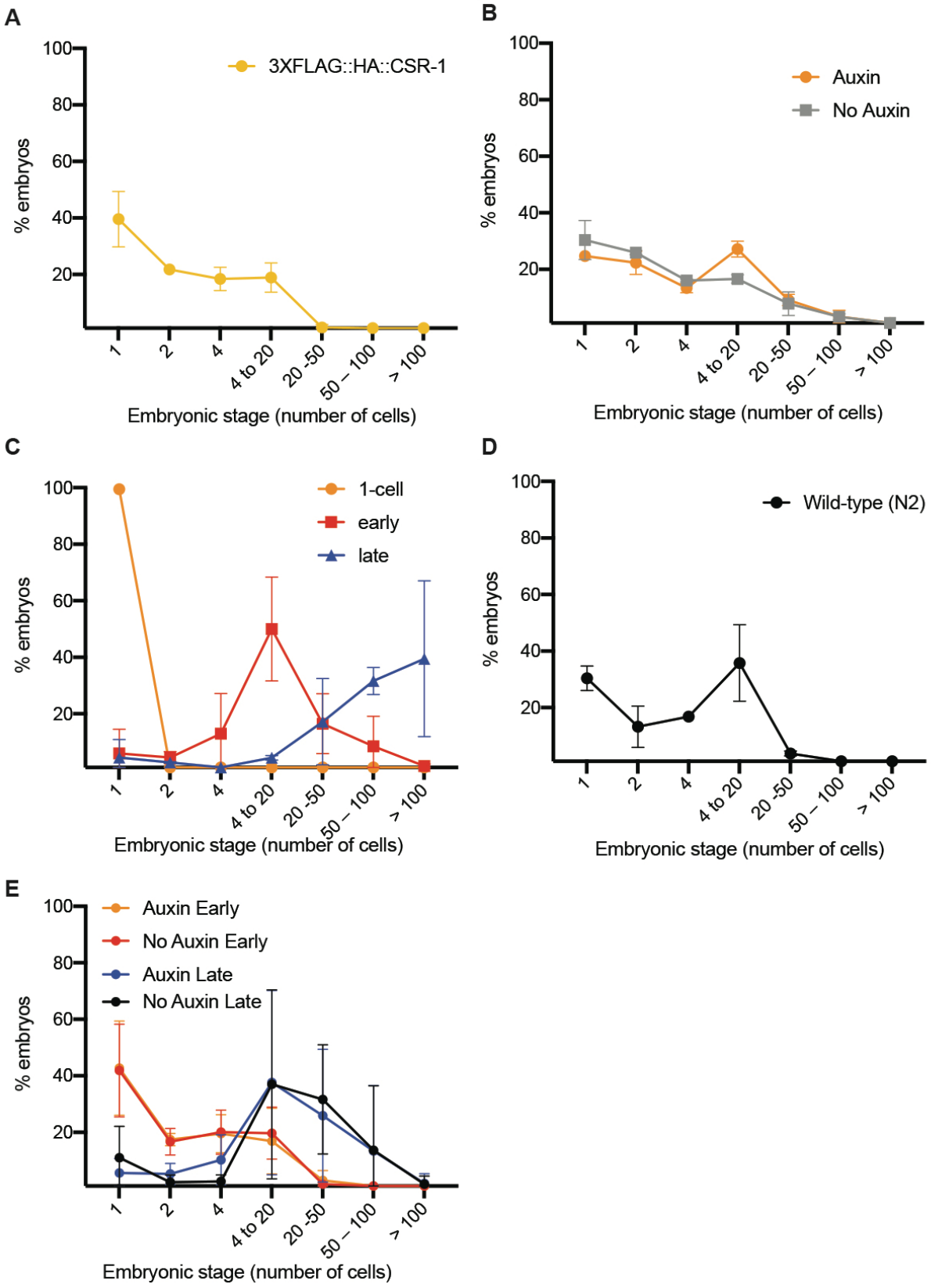
A
3XFLAG::HA::CSR-1
% embryos
100
80
60
40
20
1
2
4
4 to 20
20 -50
50 – 100
> 100
Embryonic stage (number of cells)
B
Auxin
No Auxin
% embryos
Embryonic stage (number of cells)
C
1-cell
early
late
% embryos
Embryonic stage (number of cells)
D
Wild-type (N2)
% embryos
Embryonic stage (number of cells)
E
Auxin Early
No Auxin Early
Auxin Late
No Auxin Late
% embryos
Embryonic stage (number of cells)

Fig. S4

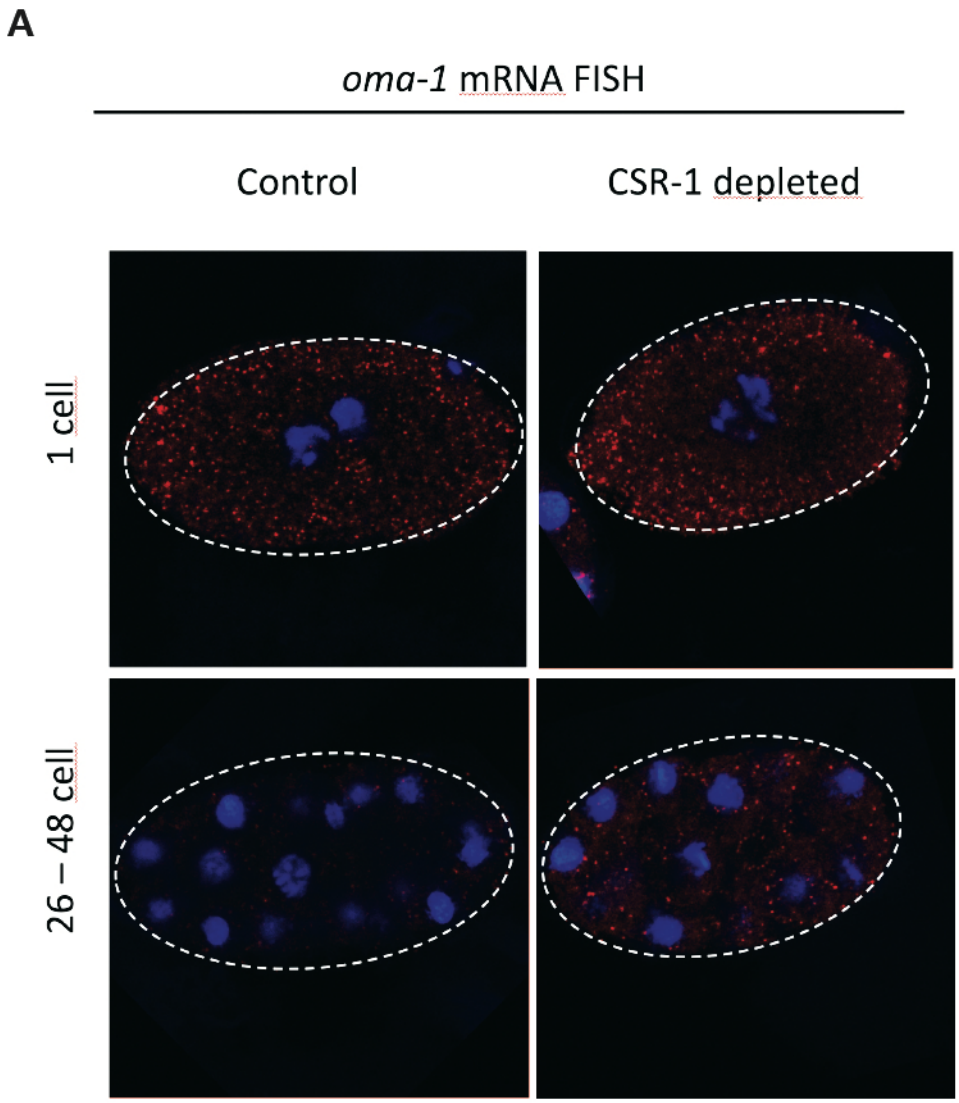

Fig. S5

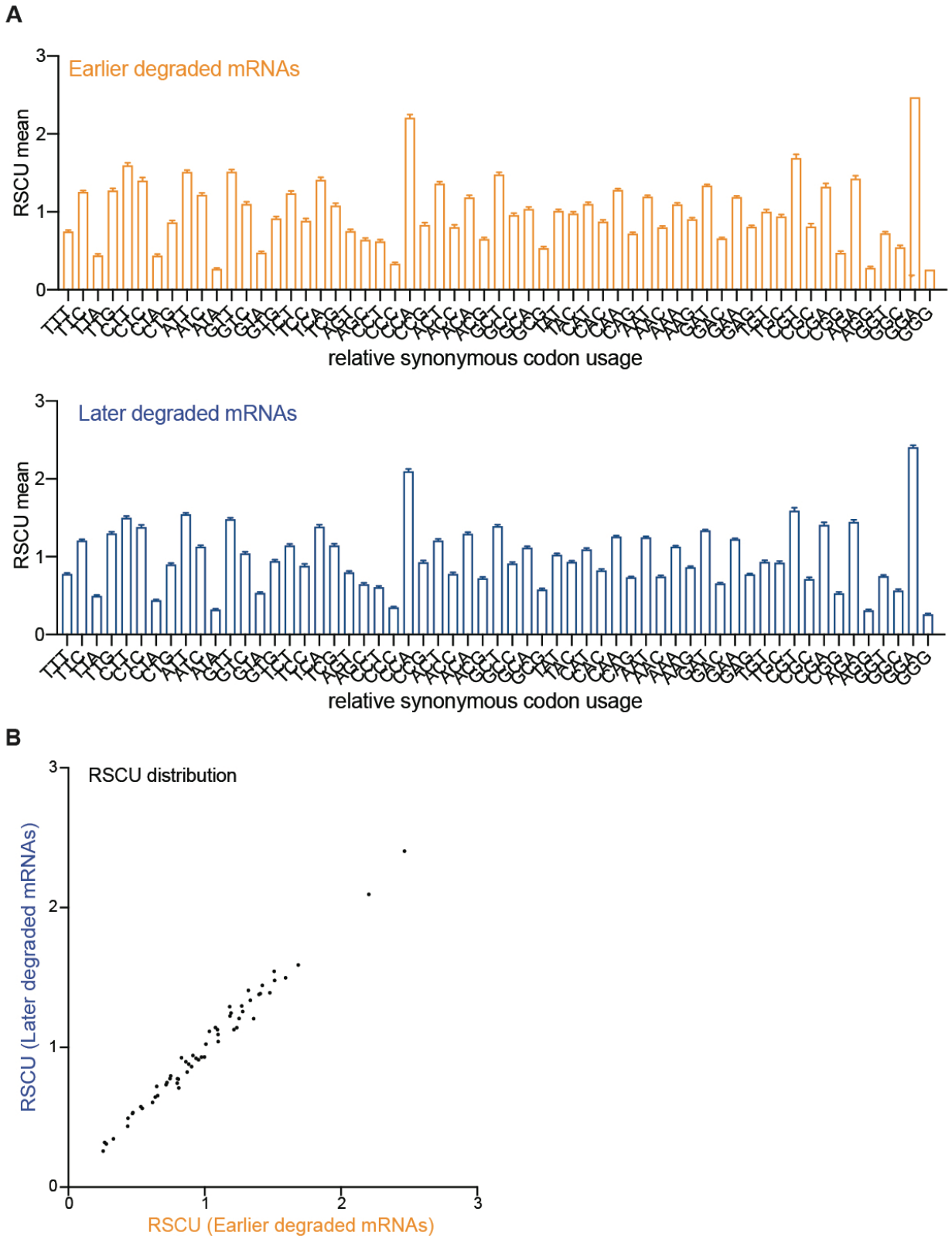
A
Earlier degraded mRNAs
RSCU mean
relative synonymous codon usage
Later degraded mRNAs
RSCU mean
relative synonymous codon usage
B
RSCU distribution
RSCU (Later degraded mRNAs)
RSCU (Earlier degraded mRNAs)